

O₂ Reduction on Graphite and Nitrogen-Doped Graphite: Experiment and Theory

Reyimjan A. Sidik and Alfred B. Anderson*

Department of Chemistry, Case Western Reserve University, Cleveland, Ohio 44106

Nalini P. Subramanian, Swaminatha P. Kumaraguru, and Branko N. Popov

Department of Chemical Engineering, University of South Carolina, Columbia, South Carolina 29208

Received: September 12, 2005; In Final Form: November 22, 2005

An experimental and theoretical study of electroreduction of oxygen to hydrogen peroxide is presented. The experimental measurements of nitrided Ketjenblack indicated an onset potential for reduction of approximately 0.5 V (SHE) compared to the onset potential of 0.2 V observed for untreated carbon. Quantum calculations on cluster models of nitrided and un-nitrided graphite sheets show that carbon radical sites formed adjacent to substitutional N in graphite are active for O₂ electroreduction to H₂O₂ via and adsorbed OOH intermediate. The weak catalytic effect of untreated carbon is attributed to weaker bonding of OOH to the H atom-terminated graphite edges. Substitutional N atoms that are far from graphite sheet edges will be active, and those that are close to the edges will be less active. Interference from electrochemical reduction of H atoms on the reactive sites is considered, and it is shown that in the potential range of H₂O₂ formation the reactive sites are not blocked by adsorbed H atoms.

Introduction

Catalyst support materials such as Vulcan XC-72R, Black Pearl 2000, Ketjenblack, and others are used in low-temperature fuel cells because of their high surface area, good chemical and mechanical stability, and good electrical conductivity,¹ but not because of catalytic properties.² The supports are known to be only weakly active toward the electroreduction of oxygen. However, Wang et al. reported making nitrogenated carbon particles that were active toward oxygen reduction.³ They oxidized Vulcan XC-72R (surface area ~250 m²/g) with 30% HNO₃ under refluxing condition, reacted the product with NH₃ at 600 °C, and then heat-treated it in Ar at 900 °C. The nitrogenated product exhibited greater catalytic activity toward oxygen reduction in sulfuric acid than the untreated carbon, and there was a 210 mV anodic shift in the oxygen reduction peak.³

Carbon–nitrogen materials prepared in other ways can be inactive toward oxygen reduction. Lalande et al.⁴ reported that CN_x particles prepared by pyrolysis of nitrogen-containing organic compounds in Ar at 1000 °C or by pyrolysis of a hydrocarbon, followed by heat treatment in NH₃ at 1000 °C, did not show any activity toward oxygen reduction.

Carbon has a long history as a support in the heterogeneous catalysis literature,⁵ and only recently have the effects of adding N been studied. For example, compared to their nondoped counterparts, some N-doped carbon particles show more oxidation resistance.⁶ Some show catalytic activities toward NO_x reduction.^{7,8} Others are oxidation catalysts.⁹ In the case of NO_x oxidation and O₂ reduction, the O₂⁻ superoxide radical was proposed to explain the enhanced activity.^{9,10} These properties have been attributed to electronic or structural changes caused by the nitrogen incorporation into the graphite layers. However,

the compositions and structures of the active sites are not yet known.

Carbon nitriles (CN_x) in thin film forms have been studied over the past decade. They possess high hardness, low coefficients of friction, chemical inertness, and low work functions.¹¹ Recently, Hellgren et al.¹² studied the electronic structures of carbon nitride thin films by using a combination of experimental electronic structure probes and density functional theory. From comparisons of experimental spectra with calculated electronic properties for different model systems, they identified three bonding structures for the nitrogen: nitrile bonds (C≡N), pyridine-like nitrogen where N bonded to two C atoms, and graphite-like N, i.e., N bonded to three C atoms, N substituting into the graphitic network. In the present paper, the last of these is referred to as “nitrided graphite” or “graphite nitride”. They also reported that thin films made by dc magnetron sputtering at low temperatures, <150 °C, were amorphous. For temperatures above 200 °C, when the N concentration was greater than 5%, the structures were fullerene-like, but for N concentrations below 5%, graphite nitride formed.¹³ The graphitic CN_x thin films exhibited better thermal stability than the films grown at low temperature.¹⁴

The mechanisms for oxygen reduction, both in the presence and in the absence of substitutional N in the graphite, and the cause of the anodic shift are not known. The catalytic effect of nitridding is a worthwhile issue to explain. To understand the mechanisms and catalytic effect, we have undertaken a quantum chemical study of nitrided graphite using a small and a large cluster model, both terminated on the edge by bonding to hydrogen atoms.

This paper reports new oxygen reduction results for nitrided Ketjen Black EC 300 J. The surface area of pristine ketjen black is 886 m²/g. A comparison of the experimental and theoretical results will be made. The comparison will indicate that two-electron oxygen reduction to hydrogen peroxide takes place on the edges of the graphite sheets or on nitrided graphite basal

* Corresponding author. E-mail aba@case.edu. Phone 216-368-5044. Fax 216-368-3006.

planes, where it is activated by radical carbon sites adjacent to substitutional N atoms in the graphite sheet. The idea that a carbon radical is involved was motivated by a previous study of hydrogen evolution over radical sites on boron-doped diamond electrodes.¹⁵ A subsurface substitutional boron atom gave a second-layer carbon atom radical character, allowing it to chemisorb an H atom weakly. This atom then participated in electrochemical H₂ evolution.¹⁵ The same is found for the OOH intermediate formed in the first step in oxygen reduction: it is stabilized by bonding to a radical carbon site that is created by the substitutional N, and its reduction forms H₂O₂. It is found that, at potentials below the OOH(ads) formation potential, the carbon radical has H bonded to it, but the H is predicted to be oxidized off at higher potentials.

Experimental Approach

Synthesis of Nitrogen-Doped Carbon. Commercially available carbon black, namely Ketjen Black EC 300 J, was treated in HCl and HNO₃ to remove the metallic impurities.^{16,17} The as-received Ketjen Black EC 300 J was pre-washed twice with 6 M HCl for 24 h. Next, the chloride impurities present in the sample were washed out with distilled water. The pre-washed carbon was subjected to oxidation in 70% HNO₃ for 7 h under reflux conditions. It was then washed in distilled water and dried in an oven at 75 °C. For brevity, as-received Ketjen Black EC-300J is denoted as K, HCl-treated carbons as K1, and HNO₃-treated carbons as K2. The HNO₃-treated carbon was subjected to heat treatment in NH₃ at 900 °C to obtain nitrogenated carbon (K3).

Electrochemical Characterization. Electrochemical characterizations were performed in a single-compartment three-electrode cell. The electrocatalytic activity of the modified carbon was studied using the rotating ring disk electrode (RRDE) technique.^{18–21} Briefly, a rotating ring disk electrode from Pine Instruments employing a glassy carbon disk (5 mm o.d.) and Pt ring (5.52 mm i.d., 7.16 o.d.) was used as the working electrode. Platinum wire was used as the counter electrode, and a standard Hg/HgSO₄ electrode was used as the reference electrode. The potentials presented in this study are referred with respect to standard hydrogen electrode (SHE). A catalytic film was produced at the disk electrode according to the following procedure: 8 mg of the modified carbon was suspended in isopropyl alcohol and ultrasonically blended for 10 min. 15 μL of this suspension was applied as an ink on the disk electrode in steps of 5 μL. A 5 μL Nafion solution [1(5 wt % Nafion)/10(water)/10(isopropyl alcohol)] was added on top of the film. 0.5 M H₂SO₄ was the electrolyte in all of the studies, and prior to measurements, the solution was purged with nitrogen. Cyclic voltammograms (CVs) were recorded by scanning the disk potential from 1.04 to 0.04 V vs SHE at a scan rate of 5 mV s⁻¹. For all electrochemical measurements, the ring potential was maintained at 1.2 V vs SHE in order to oxidize any hydrogen peroxide produced.¹⁹ First, CVs were recorded at 5 mV s⁻¹ using nitrogen atmosphere to obtain the background capacitive currents. Next, the CVs were recorded using the oxygen-saturated electrolyte. The electrolyte solution was purged with oxygen for 15 min before commencing oxygen reduction on the disk electrode. Linear sweep voltammograms for disk potentials were recorded from 1.04 to 0.04 V vs SHE at a scan rate of 5 mV s⁻¹ for different rotation rates of the RRDE. The linear sweep voltammograms shown in this paper were obtained at 900 rpm unless specified otherwise. The net faradic current was obtained by subtracting the background capacitive current from the N₂ CV.²⁰ All measurements were

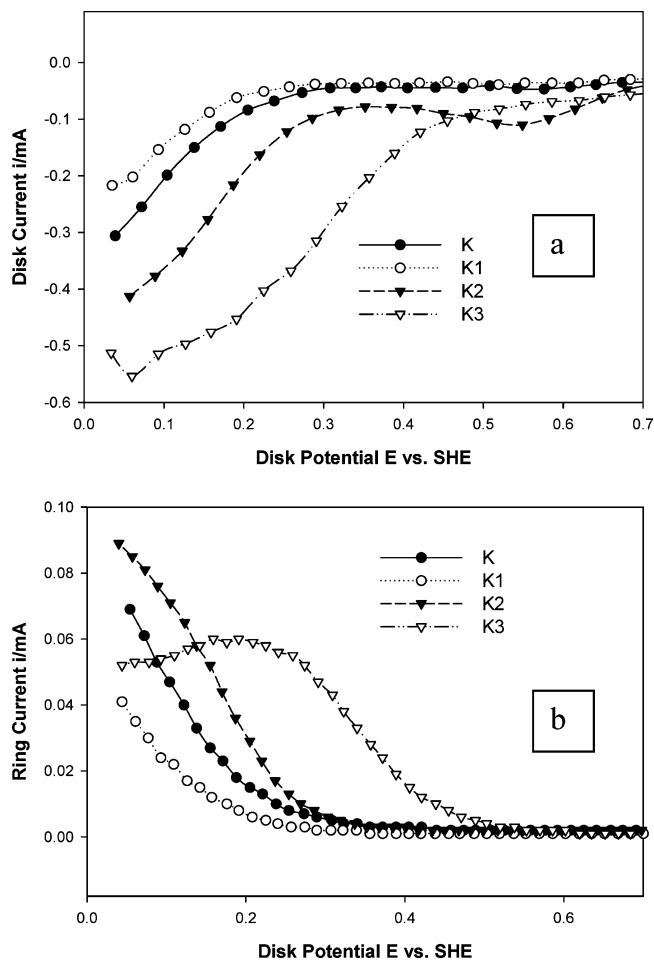


Figure 1. (a) Disk currents and (b) ring currents for modified carbons K, K1, K2, and K3 in 0.5 M H₂SO₄ solution saturated with oxygen. The linear sweep voltammograms were recorded at 5 mV/s scan rate and 900 rpm rotation rate.

obtained with a bipotentiostat (model AFRDE from Pine Instruments).

Experimental Results and Discussion

The as-received carbon (K), HCl-treated carbon (K1), HNO₃-treated carbon (K2), and nitrogenated carbon (K3) were tested for activity toward oxygen reduction. Figure 1a shows typical polarization curves for oxygen reduction by these carbons on a rotating disk electrode in 0.5 M H₂SO₄. The highest activity is for the HNO₃-treated carbon that was subjected to heat treatment in NH₃. A performance trend of K3 > K2 > K > K1 is clearly seen in Figure 1a. The as-received carbon support shows greater activity than the HCl-treated carbon, and this is attributed to the presence of metallic impurities. The HCl treatment evidently removes the metallic impurities, and K1 represents the activity of bare carbon. Oxidized carbon K2 shows about 100 mV less activation overpotential for oxygen reduction reaction compared to K1. Electrochemical analysis indicated that oxidation of carbon in nitric acid introduces oxygen, probably as quinone groups, on the carbon surface.³ The 0.55 V vs SHE peak in the linear sweep voltammograms of K2 is characteristic of the quinone–hydroquinone redox couple. The onset potential for oxygen reduction reaction is 0.3 V vs SHE. Further introduction of nitrogen, by heat treatment at 900 °C in a NH₃ atmosphere, increases the activity of the catalyst by nearly 200 mV in the anodic direction. The onset potential is as high as 0.510 V vs SHE.

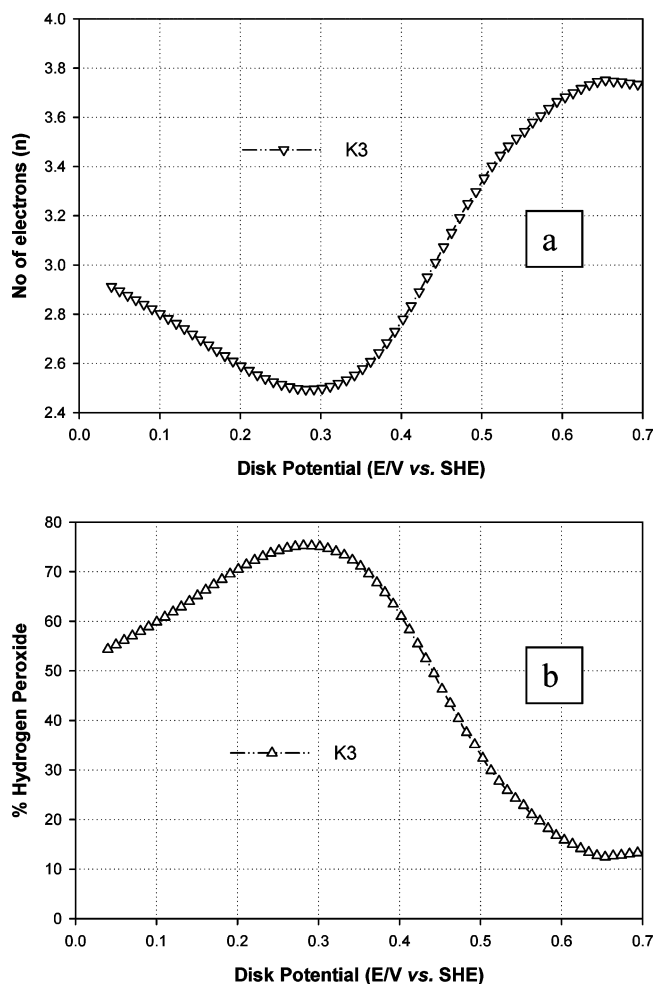


Figure 2. (a) Number (N_e) of electrons produced and (b) % H_2O_2 produced as calculated from eq 1 and eq 2 for the nitrogenated carbon K3 whose disk and ring currents are shown in Figure 1a,b.

Oxygen electroreduction in acid can be either a four-electron discharge to form water or a two-electron reduction to form peroxide. Figure 1b gives the ring currents of the carbons K, K1, K2, and K3. The ring currents were measured to estimate the amount of generated hydrogen peroxide. It can be observed that the ring currents initiate at the same potentials as the onset potentials for oxygen reduction in the disk, indicating that the generation of hydrogen peroxide is taking place. For nitrated carbon, the ring current initiates at the onset potential of 0.51 V vs SHE. Also, the bell-shaped curve of the ring current is characteristic of hydrogen peroxide produced on non-noble metal catalysts and activated carbon.²⁰ The number of electrons transferred (n) and the percentage of hydrogen peroxide produced (% H_2O_2) can be determined by the following equations:^{20,21}

$$n = 4I_D / (I_D + I_R/N) \quad (1)$$

$$\% H_2O_2 = 100(4 - n)/2 \quad (2)$$

where N , I_D , and I_R are the collection efficiency, disk current, and ring current, respectively. We assumed the collection efficiency to be a constant at an estimated value of 0.25 for all the catalysts studied. Figure 2 shows the number of electrons and % H_2O_2 generated for the nitrogenated carbon K3. The obtained values clearly indicate that oxygen reduction on the nitrogenated carbon surface becomes predominantly two-

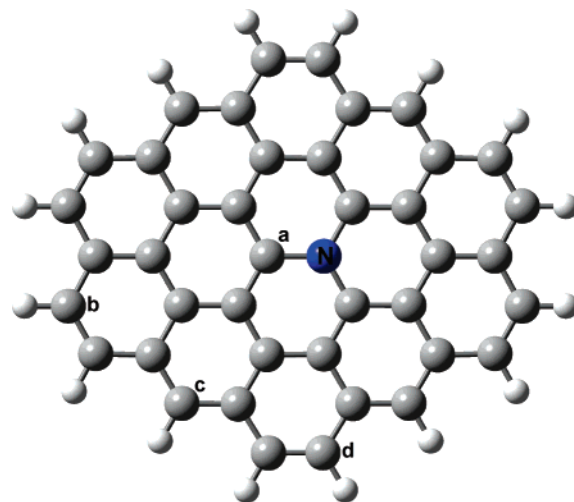


Figure 3. Optimized structure for the N-substituted graphite model, $C_{41}NH_{16}$. The larger gray circles are carbon atoms, and the smaller white circles are hydrogen atoms.

electron at higher overpotentials, leading to the production of hydrogen peroxide. At still higher overpotentials, the decrease in percentage hydrogen peroxide produced is attributed to the reduction of oxygen to water through a four-electron process or through two two-electron processes. The high O=O bond strength of 494 kJ/mol has been discussed in this context.²² The series pathway, through peroxide production and its subsequent reduction to water, and the direct four-electron pathway can occur in parallel on some surfaces, though at high overpotentials to the four-electron process. The formation of peroxide does not require the breaking of the O=O bond, but does weaken it to an O—O single bond. Further reduction to water requires that this bond be broken. Thus, on less reactive surfaces, such as the synthesized graphite and nitrated carbon, hydrogen peroxide is the reduction product.

Theoretical Method

A. Cluster Calculations. In this study, a cluster approach was used with the B3LYP hybrid density functional theory in *Gaussian 03*.²³ The basis sets used for O, N, and H were 6-31G**. Graphite models used in this work contained four and fourteen hexagonal rings with delocalized π electrons and terminated with C—H bonds. For modeling the nitrated basal plane sheet of graphite, a nitrogen atom was placed substitutionally as shown in Figure 3. Adsorption of reaction intermediates on sites a–d and others of the graphite and nitrated graphite models was examined. The bond strength values were calculated using the formula

$$BS = E(\text{cluster}) + E(\text{adsorbate}) - E(\text{adsorbate on cluster}) \quad (3)$$

B. Calculating Reversible Potentials for Forming Adsorbed Reaction Intermediates. The reversible potentials were calculated by a Gibbs linear free energy relationship.^{24,25} The essence of this free energy relationship is that, if one has the reversible potential for a redox reaction in solution bulk, then the electrode surface value can be approximated as a perturbation to this because of bonding to the surface. It is assumed that when the intermediates are bonded to the surface the solvation interactions of the reactants and the products of the electron transfer are equally reduced. Thus, the adsorption bond strengths may be used to make predictions of reversible potentials. As

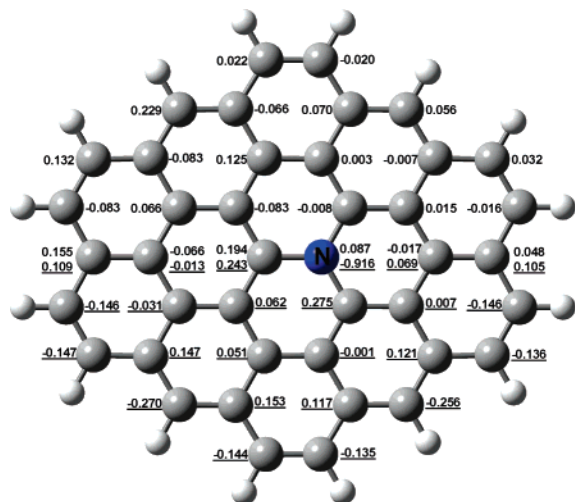


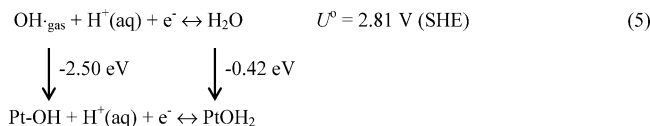
Figure 4. Spin and charge distributions for $C_{41}NH_{16}$ in its optimized structure. Both values are shown along the symmetry axis. The first number in each pair refers to the spin density, and the underlined numbers refer to the charge density. The cluster is symmetric, so spin densities are given on the top half and charge densities are given on the bottom half. For the edge H atoms, the spin and charge densities are, on average, <0.001 and ~ 0.085 , respectively, and they are not shown.

an example, consider OH reduction in solution and on the Pt surface. The reversible potential for forming the intermediate on the electrode surface is

$$U_{\text{surface}}^{\circ} = U^{\circ} + (\text{product adsorption bond strength} - \text{reactant adsorption bond strength})/F \quad (4)$$

where F is the Faraday constant.

The bulk and surface reactions can be related in a reaction cycle



The reversible potential for the onset of the surface process is then given by

$$U_{\text{surface}}^{\circ} = 2.81 + -2.50 + 0.42 = 0.73 \quad (6)$$

where 2.81 V is the experimental reversible potential for the water oxidation and OH reduction in acid solution, and 2.50 and 0.42 eV are the respective measured adsorption bond strengths for OH^{26} and H_2O^{27} at low coverage. The predicted water oxidation onset potential of 0.73 V on Pt is within 0.2 V of the observed value of 0.55 V in acid in the absence of anion adsorption.²⁸

Theoretical Results and Discussion

A. Adsorption Energies for H, O_2 , OOH, and H_2O_2 on the Radical Sheet Cluster $C_{41}NH_{16}$ and on $C_{42}H_{16}$. Figure 3 shows the fully optimized geometry for the 14-ring $C_{41}NH_{16}$ sheet radical in the absence of an adsorbate and in the doublet state. It has a C_{2v} symmetry along the C_a -N axis and is flat with no more than $\pm 0.001 \text{ \AA}$ variations from planarity. Because of the symmetric distribution of spin and charge densities along the C_a -N axis, the display may be simplified: The top half of Figure 4 shows only spin densities, while both spin and charges are shown along the C_a -N axis, and at the bottom half, only

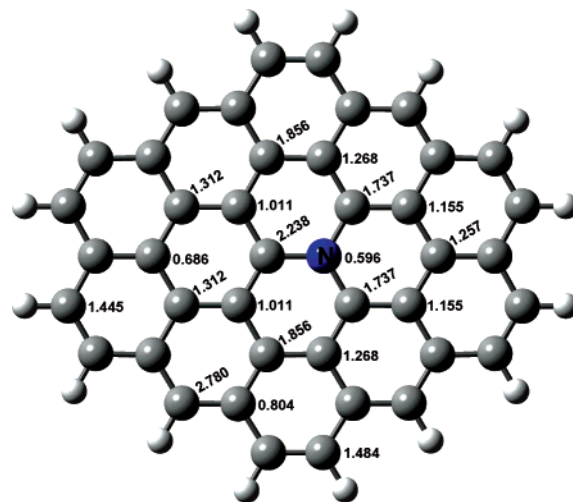


Figure 5. H adsorption bond strengths (eV) to $C_{41}NH_{16}$ as a function of position. Note that the cluster symmetry makes the H bond strength distribution symmetric.

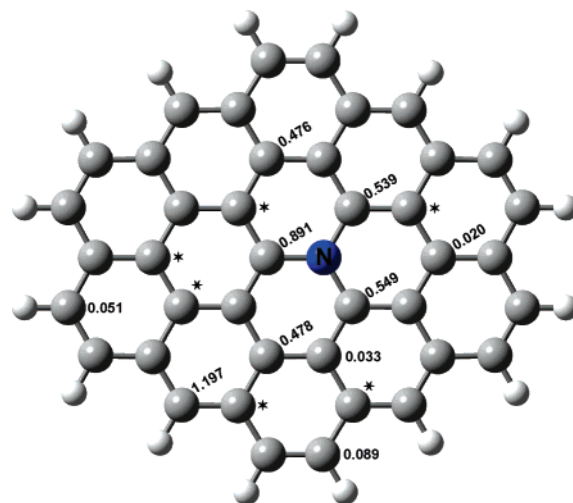


Figure 6. OOH adsorption bond strengths (eV) to $C_{41}NH_{16}$ as a function of position. The “*” means that the calculation for that site did not converge.

the charge densities are shown. The N atom is quite negative, with a charge of -0.916 . This is a consequence of N being a radical and more electronegative than carbon. Most of the compensating positive charge is distributed on the three neighboring carbon atoms. The spin density due to the unpaired electron is seen in Figure 4 to delocalize onto adjacent C atoms mostly on the left side of the N atom, with the highest spin densities found on the edge C atom c (defined in Figure 3) and its symmetric counterpart.

As expected, the optimized geometry of the pure graphene sheet, $C_{42}H_{16}$, is perfectly planar. A spin-unrestricted calculation revealed no spin polarization.

The adsorption bond strengths for H and OOH on $C_{41}NH_{16}$ used in this study are shown for several adsorption sites in Figure 5 and Figure 6, respectively. In Figure 7, it is shown that the adsorption bond strengths of adsorbate radicals, H and OOH, exhibit a correlation with the spin density only when the net spin is >0.1 . The highest bond strengths within the cluster for H and OOH are 2.238 and 0.891 eV, respectively, on the carbon atom that is directly bonded to N. Structures are shown in Figure 8a,b. When a radical adsorbs on the radical sheet, the changes in the hybridization of the adsorption site atoms distort the planar geometry, raising the adsorption site carbon out of the plane

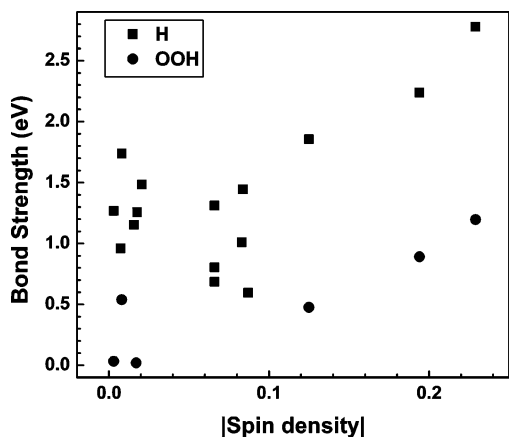


Figure 7. Bond strengths as functions of spin density for H and OOH bonded to various sites on $C_{41}NH_{16}$.

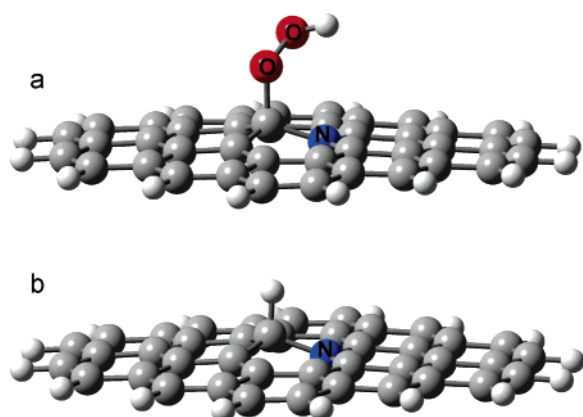


Figure 8. Optimized structures for OOH (a) and H (b) when bonded adjacent to the substitutional N in $C_{41}NH_{16}$. Upon adsorption of OOH or H, the flat 14-ring sheet adopts a concave geometry.

toward a tetrahedral structure. If the adsorbate is bonded to an edge carbon atom, it is able to relax to a nearly tetrahedral structure. The adsorption bond strengths of the neutral molecules O_2 and H_2O_2 on the radical sheet are very weak, and the planar geometry of the sheet radical is not significantly affected.

Bond strengths to carbon atoms on the edges of $C_{41}NH_{16}$ took a range of values. For sites labeled **b**, **c**, and **d**, the respective bond strengths of H are 1.445, 2.780, and 1.484 eV, and for OOH, they are 0.051, 1.197, and 0.089 eV. When H is bonded to edge site **c**, it forms a C–H bond that is stronger than the bond it forms to the carbon atom at site **a**, adjacent to substitutional N. OOH bonds by 1.197 eV to edge site **c**, which is also stronger than its bonding to site **a**. The strong bonding at the edge of the nitrated cluster is caused in part by the flexibility of edge sites to adopt the tetrahedral structure and, as will be shown below, the spin density on the site **c** carbon in the nitrated cluster, which is absent in the case of the undoped cluster. The two H atoms in the methylene group are symmetrically distributed above and below the sheet plane, while the neighboring C and H atoms are nearly unmoved. A similar structure was adopted in the case of OOH adsorption on the edge site **c**.

To understand better the effect of the substitutional N on the adsorption bond strength of H and OOH radicals, we calculated adsorption bond strengths for sites **a–d** on the undoped graphite sheet, $C_{42}H_{16}$. The results are shown in Figure 9. For both radicals, the undoped graphite sheet has stronger adsorption bonds at the edge than at the center, just like the nitrated counterpart. However, the bonding is weaker on the undoped

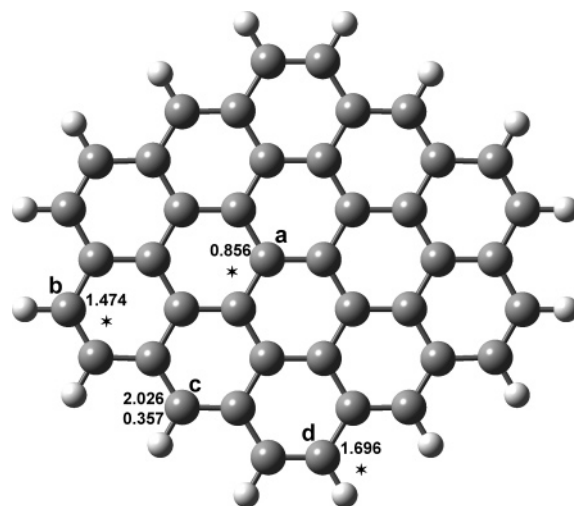


Figure 9. The H (first number) and OOH (second number) radical adsorption bond strengths (eV) on the pure graphite sheet, $C_{42}H_{16}$. The “*” means that the calculation for that site did not converge.

TABLE 1: Reversible Potentials for Reactions Used in This Work

reactions	U° (V/SHE)
$H^+(aq) + e^- (U^\circ) \leftrightarrow H(aq)$	-2.11^a
$O_2(g) + H^+(aq) + e^- (U^\circ) \leftrightarrow OOH(aq)$	-0.046^b
$OOH(aq) + H^+(aq) + e^- (U^\circ) \leftrightarrow H_2O_2(aq)$	1.436^b

^a ref 32. ^b ref 30.

graphite sheet. These bond strengths will next be used to explain the catalytic abilities of the doped and undoped graphite.

B. Reversible Potentials for Oxidation of H and O_2 Reduction Intermediates. Graphite. For all the reversible potential calculations in this paper, the values for bulk reactions in Table 1 were used in eq 6. The adsorption energies of nonradical reactants and products were taken as zero. The resulting predicted reversible potentials for forming H on the undoped $C_{42}H_{16}$ cluster model are -1.254 V, -0.636 V, -0.084 V, and -0.414 V for H on sites **a–d**, respectively. The value 0.311 V is predicted for OOH formation on the edge site **c**, and this appears to be the cause of the observed current onset potential on Ketjenblack in Figure 1a. The reversible potential for the OOH reduction step will be 1.097 V, which is much greater than 0.311 V. This value is based on assigning values of zero to the adsorption bond strengths of the O_2 reactant and the H_2O product molecules and the realization that any errors in the adsorption bond strengths of the intermediates cancel out.²⁹ In this case, OOH is the adsorbed intermediate for the first and second reduction steps. The standard reversible potential for hydrogen peroxide formation is 0.695 V.³⁰ Given these conditions, the sum of the two one-electron reversible potentials divided by 2 will be 0.695 V, which is the reversible potential for the overall two-electron process. The second step can take place at any potential less than 1.079 V, and so the first step determines the overpotential in this case according to this simple picture. It is obvious that the ideal situation for a reaction where several electrons are transferred is for the reversible potential for each electron-transfer step to equal the reversible potential for the overall multielectron reaction.²⁹ The electron-transfer activation energies will also contribute to the overpotential, as will be evident in the Tafel plot.³¹ It is important that edge sites be available for reaction at this potential, and not blocked by adsorbed H. They are available,

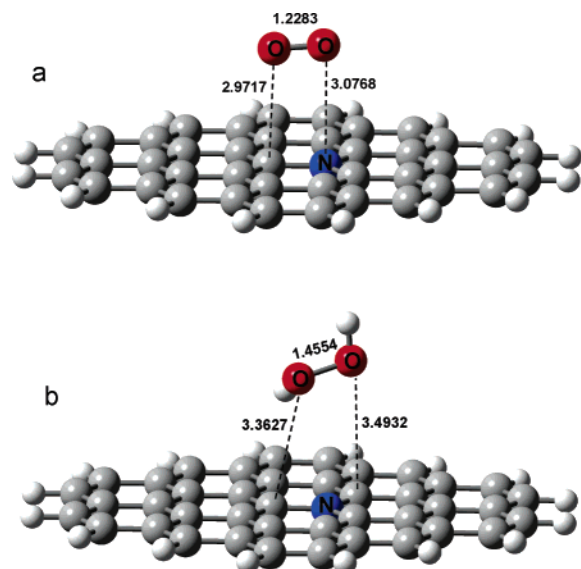


Figure 10. Optimized structures for O₂ (a) and H₂O₂ (b) when bonded adjacent to the substitutional N in C₄₁NH₁₆.

because according to the calculated reversible potentials, H(ads) will be unstable to oxidative removal in the potential range of interest.

Graphite Nitride. As can be seen from Figure 5, the highest bond strength site for H adsorption on the nitrated cluster lies at the edge site c, where the bond strength is 2.780 eV. The reversible potential for the oxidation of this H is 0.67 V, based the reversible potential for the reduction of H⁺(aq), -2.11 V.³² This potential is too high to account for the observed current onset potential in Figure 1a, where O₂ reduction occurs below 0.67 V. This means that in the 14-ring model the N is too close to the edge, and hence, we conclude that N near a graphite edge will not generate activity. However, when there is no edge site nearby, a C atom adjacent to N is a candidate for being an active site. Of the nonedge sites, it has the highest bond strength for H, and the reversible potential for its oxidation is 0.128 V, which is a good potential for maintaining an active radical site for O₂ reduction.

For the centrally located substitutional N, the spin density is highest on the site a carbon neighboring the N, but other atoms have nonzero spin densities, so adsorption bond strength for reaction intermediates O₂, OOH, and H₂O₂ were calculated on some of the other sites too. The interactions of O₂ and H₂O₂ with all sites are very weak, with the highest adsorption bond strengths on the nonedge sites being 0.056 and 0.076 eV, respectively. For the edge sites, the respective results are 0.036 and 0.179 eV. The structure perturbations to the cluster caused by the weak bonds are small, as shown in Figure 10. Bond strengths for OOH on the nitride cluster, as may be seen in Figure 6, range from 0.02 to 1.197 eV, depending on the adsorption site. The most stable edge site is c, just as for H adsorption. By using the highest adsorption bond strength values for OOH, the reversible potentials in Table 2 were obtained for the formation of H₂O₂ from O₂ reduction in acidic solution. The calculated reversible potential for the overall reaction is the same as the reported standard experimental values of 0.695 V, because as mentioned earlier, (i) the reversible potential for the overall reaction does not depend on the adsorption bond strength of the OOH reaction intermediate, and (ii) the adsorption energies of the O₂ reactant and H₂O₂ product are taken as zero. As shown in Table 2, for the edge site c, the second electron-transfer step has a reversible potential of 0.239 V, which

TABLE 2: Predicted Reversible Potentials for O₂ Reduction on the 14-Ring Radical Cluster, C₄₁NH₁₆

reaction	U ^o (V/SHE)	
	on edge C (site c)	on C adjacent to N
O ₂ (g) + H ⁺ (aq) + e ⁻ (U ^o) ↔ OOH(ads)	1.151	0.845
OOH(ads) + H ⁺ (aq) + e ⁻ (U ^o) ↔ H ₂ O ₂ (aq)	0.239	0.545
overall reaction		
O ₂ (g) + 2H ⁺ (aq) + e ⁻ ↔ H ₂ O ₂ (aq)	0.695	0.695

TABLE 3: Adsorption Bond Strengths, D_e (eV), for H and OOH on the Adjacent Site Carbon and the Highest Bond Strength Edge Site on the 4-Ring and 14-Ring Model Systems with N in the Center

adsorbate	adjacent site			highest D _e edge site			
	4 ring	14 ring	Δ ^a	4 ring	14 ring	(no N)	Δ ^a
H	2.315	2.238	-0.077	3.000	2.780	(2.026)	-0.220
OOH	0.903	0.891	-0.039	1.566	1.197	(0.357)	-0.369

$$^a \Delta = D_e(14 \text{ ring}) - D_e(4 \text{ ring}).$$

is too low to account for the experimental current onset potential for H₂O₂ formation in Figure 1a. However, using the highest bond strength, 0.891 eV, which is for OOH on the site adjacent to N, respective reversible potentials 0.845 and 0.545 V are predicted for the first and second electron-transfer steps. The second matches the observed current onset potentials for H₂O₂ generation on nitrogenated Ketjenblack quite well, as shown by the curve labeled K3 in Figure 1a.

The spatial extent of the influence of the substitutional N atom is of interest. Calculations of H and OOH bond strengths to a smaller four-ring cluster were made. As is evident from Table 3, bond strengths to C adjacent to N in a 4-ring C₁₅NH₁₀ cluster increased very little, but the bond strengths at the edge sites increased somewhat more. The bond energies to the edge of the undoped 14-ring cluster approximates the limit for large clusters and the limit of substitutional N being far from an edge. These values are in the column labeled "no N". The bond energies indicate that the biggest perturbation effect of N is local, but when the N is near an edge, it magnifies the reactivity of edge sites toward bonding radical molecules to the extent that they will be passivated against oxygen reduction activity at the potentials shown in Figure 1a, curve K3.

Conclusions

Nitrated carbon obtained from oxidized carbon that is heat-treated in NH₃ at 900 °C shows a high 0.510 V vs SHE onset potential toward oxygen reduction. Oxygen reduction is predominantly by the two-electron process to hydrogen peroxide, as observed from RRDE studies. Quantum calculations show that carbon radical sites formed adjacent to substitutional N in graphite are active for O₂ electroreduction to H₂O₂ in acid electrolyte, and this may explain the catalytic effect observed for nitrated carbon. Furthermore, the weak catalytic effect of untreated carbon can be attributed to the weaker bonding of the OOH(ads) reaction intermediate to H atom-terminated graphite edge sites. Substitutional N atoms that are far from the graphite sheet edges will be active, and those that are close to the edges will be less active.

Acknowledgment. This work was supported by the Department of Energy through grant no. DE-FC36-03GO13108.

References and Notes

- (1) Kinoshita, K. *Carbon: Electrochemical and Physicochemical Properties*; John Wiley & Sons: New York, 1988.
- (2) Hossain, M. S. Oxygen reduction on carbon and modified carbon surfaces. Ph.D. Dissertation, Case Western Reserve University, Cleveland, OH, 1986.
- (3) Wang, H.; Côté, R.; Faubert, G.; Guay, D.; Dodelet, J. P. *J. Phys. Chem. B* **1999**, *103*, 2042.
- (4) Lalonde, G.; Côté, R.; Guay, D.; Dodelet, J. P.; Weng, L. T.; Bertrand, P. *Electrochim. Acta* **1997**, *42*, 1379.
- (5) Radovic, L.; Rodriguez-Reinoso, F. Carbon Material in Catalysis. *Chem. Phys. Carbon* **1997**, *25*, 243.
- (6) Mang, D.; Boehm, H. P.; Stanczyk, K.; Marsh, H. *Carbon* **1992**, *30*, 391.
- (7) Huang, M.; Teng, H. *Carbon* **2003**, *41*, 951.
- (8) Matzner, S.; Boehm, H. P. *Carbon* **1998**, *36*, 1697.
- (9) Stöhr, B.; Boehm, H. P.; Schlögl, R. *Carbon* **1991**, *29*, 707.
- (10) Maldonado, S.; Stevenson, K. J. *J. Phys. Chem. B* **2005**, *109*, 4707.
- (11) For a recent review, see Muhl, S.; Medez, J. M. *Diamond Relat. Mater.* **1999**, *8*, 1809.
- (12) Hellgren, N.; Guo, J. H.; Luo, Y.; Sathe, C.; Agui, A.; Kashtanov, S.; Nordgren, J.; Agren, H.; Sundgren, J. E. *Thin Solid Films* **2005**, *471*, 19.
- (13) Hellgren, N.; Johansson, M. P.; Broitman, E.; Hultman, L.; Sundgren, J. E. *Phys. Rev. B* **1999**, *59*, 5162.
- (14) Hellgren, N.; Lin, N.; Broitman, E.; Serin, V.; Grillo, S. E.; Twisten, R.; Petrov, I.; Colliex, C.; Hultman, L.; Sundgren, J. E. *J. Mater. Res.* **2001**, *16*, 3188.
- (15) Cai, Y.; Anderson, A. B.; Kostadinov, L. N.; Angus, J. C. *Electrochem. Solid State Lett.* **2005**, *8*–9, E62.
- (16) Faubert, G.; Côté, R.; Dodelet, J.-P.; Lefèvre, M.; Bertrand *Electrochim. Acta* **1999**, *44*, 2589.
- (17) Hyeon, T.; Han, S.; Sung, Y.-E.; Park, K.-W.; Kim, Y.-W. *Angew. Chem., Int. Ed.* **2003**, *42*, 4352.
- (18) Claude, E.; Addou, T.; Latour, J.-M.; Aldebert, P. *J. Appl. Electrochem.* **1998**, *28*, 57.
- (19) Antoine, O.; Durand, R. *J. Appl. Electrochem.* **2000**, *30*, 839.
- (20) Marcotte, S.; Villers, D.; Guillet, N.; Roué, L.; Dodelet, J.-P. *Electrochim. Acta* **2004**, *50*, 179.
- (21) Lefèvre, M.; Dodelet, J.-P. *Electrochim. Acta* **2003**, *48*, 2749–2760.
- (22) Adzic, R. In *Electrocatalysis*; Lipkowski, J., Ross, P. N., Eds.; Wiley-VCH: New York, 1998.
- (23) Frisch, M. J.; Trucks, G. W.; Schlegel, H. B.; Scuseria, G. E.; Robb, M. A.; Cheeseman, J. R.; Montgomery, J. A., Jr.; Vreven, T.; Kudin, K. N.; Burant, J. C.; Millam, J. M.; Iyengar, S. S.; Tomasi, J.; Barone, V.; Mennucci, B.; Cossi, M.; Scalmani, G.; Rega, N.; Petersson, G. A.; Nakatsuji, H.; Hada, M.; Ehara, M.; Toyota, K.; Fukuda, R.; Hasegawa, J.; Ishida, M.; Nakajima, T.; Honda, Y.; Kitao, O.; Nakai, H.; Klene, M.; Li, X.; Knox, J. E.; Hratchian, H. P.; Cross, J. B.; Bakken, V.; Adamo, C.; Jaramillo, J.; Gomperts, R.; Stratmann, R. E.; Yazyev, O.; Austin, A. J.; Cammi, R.; Pomelli, C.; Ochterski, J. W.; Ayala, P. Y.; Morokuma, K.; Voth, G. A.; Salvador, P.; Dannenberg, J. J.; Zakrzewski, V. G.; Dapprich, S.; Daniels, A. D.; Strain, M. C.; Farkas, O.; Malick, D. K.; Rabuck, A. D.; Raghavachari, K.; Foresman, J. B.; Ortiz, J. V.; Cui, Q.; Baboul, A. G.; Clifford, S.; Cioslowski, J.; Stefanov, B. B.; Liu, G.; Liashenko, A.; Piskorz, P.; Komaromi, I.; Martin, R. L.; Fox, D. J.; Keith, T.; Al-Laham, M. A.; Peng, C. Y.; Nanayakkara, A.; Challacombe, M.; Gill, P. M. W.; Johnson, B.; Chen, W.; Wong, M. W.; Gonzalez, C.; Pople, J. A. *Gaussian 03*, revision B.04; Gaussian, Inc.: Pittsburgh, PA, 2003.
- (24) Anderson, A. B.; Roques, J. *J. Electrochem. Soc.* **2004**, *151*, E85.
- (25) Anderson, A. B.; Albu, T. V. *J. Electrochem. Soc.* **2000**, *147*, 4229.
- (26) Mooney, C. E.; Anderson, L. C.; Lunsford, J. H. *J. Phys. Chem.* **1993**, *97*, 2505.
- (27) Sexton, B. A.; Hughes, A. E. *Surf. Sci.* **1984**, *140*, 227.
- (28) Markovic, N. M.; Adzic, R. R.; Cahan, B. D.; Yeager, E. B. *J. Electroanal. Chem.* **1994**, *377*, 249.
- (29) Schweiger, H.; Vayner, E.; Anderson, A. B. *Electrochem. Solid State Lett.* **2005**, *8*, A585.
- (30) Taken from or derived from data given by Hoare, J. P. In *Standard Potentials in Aqueous Solution*; Bard, A. J., Parsons, R., Jordan, J., Eds.; Marcel Dekker: New York, 1985.
- (31) Anderson, A. B.; Roques, J.; Mukerjee, S.; Murthi, V. S.; Markovic, N. M.; Stamenkovic, V. *J. Phys. Chem. B* **2005**, *109*.
- (32) Anderson, A. B.; Kang, D. B. *J. Phys. Chem. A* **1998**, *102*, 5993.